Methods for Identifying and Tracking Phase Singularities in Computational Models of Re-entrant Fibrillation

Ekaterina Zhuchkova[1] and Richard Clayton[2]

[1] Physics Faculty, Moscow State University, Leninskie Gory,
119992, Moscow, Russia
zhkatya@polly.phys.msu.ru
http://polly.phys.msu.ru/~zhkatya/
[2] Department of Computer Science, University of Sheffield, Regent Court,
211 Portobello Street, Sheffield, S1 4DP, UK
r.h.clayton@sheffield.ac.uk
http://www.dcs.shef.ac.uk/~richard

Abstract. The dangerous cardiac arrhythmias of tachycardia and fibrillation are most often sustained by re-entry. Re-entrant waves rotate around a phase singularity, and the identification and tracking of phase singularities allows the complex activity observed in both experimental and computational models of fibrillation to be quantified. In this paper we present preliminary results that compare two methods for identifying phase singularities in a computational model of fibrillation in 2 spatial dimensions. We find that number of phase singularities detected using each method depends on choosing appropriate parameters for each algorithm, but that if an appropriate choice is made there is little difference between the two methods.

1 Introduction

Cardiac cells are electrically excitable and a propagating sequence of electrical activation and recovery (the cardiac action potential) initiates the contraction and relaxation of cardiac tissue. During normal beats the cardiac pacemaker synchronizes the electrical and mechanical activity of the heart, but during an arrhythmia the electrical activity is self-sustaining. An excitation wave that propagates repeatedly along a closed path is termed re-entry, and re-entry is the mechanism that is believed to sustain many cases of the dangerous cardiac arrhythmias of ventricular tachycardia (VT), and ventricular fibrillation (VF). In a two-dimensional tissue sheet without any obstacles a single re-entrant wave adopts a spiral shape, and in three-dimensional tissue the wave adopts a scroll shape [1]. Mapping electrical activity on the surface of the ventricles during VF has revealed complex spatio-temporal activity [2], and direct evidence of re-entrant waves is seen only rarely [3]. This is attributed either to breakdown of re-entrant waves into multiple interacting wavelets or intermittent conduction of waves emanating from a mother rotor [4-6].

One of the ways to simplify the complex activity observed during experimental studies is to identify the tips of re-entrant waves on the heart surface, and this can be

A.F. Frangi et al. (Eds.): FIMH 2005, LNCS 3504, pp. 246 – 255, 2005.

done by transforming the measured voltage distribution measured on the heart surface into phase [7, 8]. The tips of re-entrant spiral waves are surrounded by tissue in all phases of the activation-recovery cycle, and hence are phase singularities (PS). In an experimental study the phase singularities observed on the surface of ventricular tissue are intersections of filaments of PS around which re-entrant scroll waves rotate. Modeling studies show that filaments may be contained within the ventricular wall and intersect with the heart surface only briefly; this observation may explain the short lifetimes of PSs on the heart surface [9, 10].

Identification of PSs is a powerful technique for analyzing experimental data because the voltage signals recorded optically from the heart surface are often noisy, but transformation of voltage into phase removes the noise and enables accurate location of phase singularities [11]. PSs also provide a valuable link between experimental data and computational simulation [12]. However, different investigators have used different approaches to identify the location of PSs, and little is known about the differences between these methods [11-14]. In addition, although the tip trajectories of single spiral waves have been studied extensively in computational models with different parameter regimes [15], little is known about how PSs behave during the breakdown of a single re-entrant wave into fibrillation. The aim of this paper is to present preliminary results comparing two different approaches for locating PSs, and then to track phase singularities during the breakdown of a spiral wave into fibrillation.

2 Methods for Identifying Phase Singularities

In experimental studies the spatial distribution of phase has been used to identify PSs [7]. In computational studies more information is generally available, and PSs can be identified from the intersection of isolines of constant membrane voltage V_m and another variable associated with repolarisation such as a gating variable for the Ca^{2+} channel [16] or a line where $dV_m/dt = 0$ [13].

The spatial distribution of membrane voltage obtained from an experimental preparation or computational model can be mapped to a spatial distribution of phase by obtaining the current value of membrane voltage at each point $V_m(t)$ and a previous value of the membrane voltage $V_m(t\text{-}tau)$. If the delay *tau* is chosen to be a few ms, then a plot of $V_m(t\text{-}tau)$ against $V_m(t)$ for a spiral wave shows that the points follow a trajectory around a central reference point (Fig.1). If the coordinates $(V_{ref,x}, V_{ref,y})$ of the central reference point are obtained, then the phase at each point is the elevation above the V_m axis, and is given by [11]

$$phi(t) = \arctan\left[\frac{V_m(t-tau) - V_{ref,y}}{V_m(t) - V_{ref,x}}\right], \tag{1}$$

where **arctan** returns a value between –pi and +pi. Fig.2 shows the spiral wave simulation used to create the plot shown in Fig.1, together with the phase distribution obtained from Fig.1 using the mean value of V_m to give both $V_{ref,x}$, and $V_{ref,y}$.

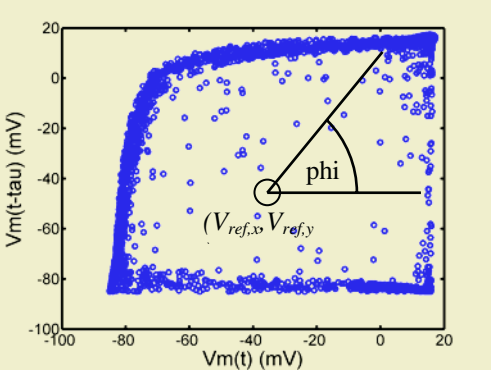

Fig. 1. Plot of $V_m(t\text{-}tau)$ vs $V_m(t)$ for a single spiral wave with a time delay *tau* of 5 ms. The phase angle *phi* is obtained for each point using the central reference point with co-ordinates $(V_{ref,x}, V_{ref,y})$ as shown

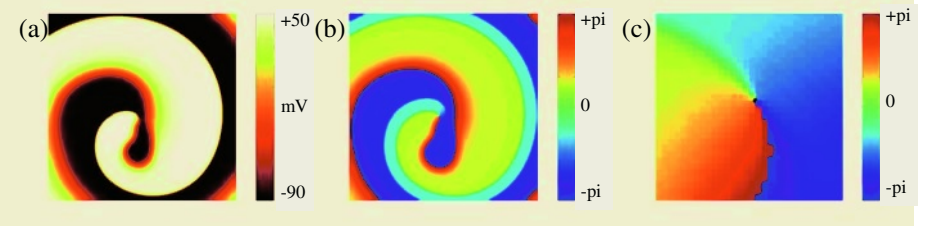

Fig. 2. Phase analysis of a single re-entrant spiral wave in a computational model (see text for details). (a) Distribution of membrane voltage. (b) Distribution of phase, obtained using a time delay of 5 ms. (c) Magnification of (b) showing the distribution of phase around the spiral wave tip and the phase singularity as a black point

As noted above, this approach is particularly useful for noisy experimental data, where the phase calculation acts as a filter to remove the noise. Different techniques can be used to identify phase singularities from the phase distribution, but all rely on identifying points that are surrounded by a complete cycle of phase from –pi to +pi [8, 11, 14]. The method used here is based on the concept of topological charge, n_t, and is described in detail elsewhere [8, 11, 14]. The mathematical definition of a PS is

$$n_t = \frac{1}{2\pi} \oint_C \nabla phi \cdot \overrightarrow{dl} \tag{2}$$

where the line integral is taken over the path $\vec{l}$ on a closed curve *C* surrounding the singularity; n_t is an integer value with the sign depending on the chirality of phase surrounding PS. The integral (2) at location $[m,n]$ can be evaluated by the following convolution operation

$$\oint_C \nabla phi.\vec{dl} \propto \nabla_x \otimes k_y + \nabla_y \otimes k_x \tag{3}$$

where $\otimes$ is a convolution operator, ∇_x and ∇_y are convolution kernels

$$\nabla_x = \begin{bmatrix} +1 & -1 \\ 0 & 0 \end{bmatrix} \qquad \nabla_y = \begin{bmatrix} -1 & 0 \\ +1 & 0 \end{bmatrix}, \tag{4}$$

and

$$\begin{aligned} k_x[m+1/2,n] &= phi[m+1,n] - phi[m,n] \\ k_y[m,n+1/2] &= phi[m,n+1] - phi[m,n] \end{aligned}. \tag{5}$$

Equation (3) provides a way to obtain a two-dimensional array from the phase distribution, and phase singularities are defined as the nonzero elements in this array.

Using the second technique a PS can be determined as the intersection point of an isoline of constant membrane voltage $V_m = V_{iso}$ and a line where $dV_m/dt = 0$ [13]. So, at timesteps n and $n+1$ the membrane voltage at a point should satisfy

$$\begin{cases} V_m^n = V_{iso} \\ V_m^{n+1} = V_{iso} \end{cases}$$

The elements of the membrane voltage array that are in accord with these two simultaneous equations then designate phase singularities.

3 Cardiac Virtual Tissue

The cardiac virtual tissue used in this study was a simplified 2D model of a sheet of ventricular tissue, where action potential propagation was described using a monodomain formulation

$$\frac{\partial V_m}{\partial t} = D\left(\frac{\partial^2 V_m}{\partial x^2} + \frac{\partial^2 V_m}{\partial y^2}\right) - \frac{1}{C_m} I_{ion}, \tag{6}$$

where D denotes a diffusion coefficient, C_m the specific membrane capacitance, and I_{ion} current flow through the cell membrane [17]. We used the three variable model described by Fenton and Karma to compute I_{ion}, with parameters set to reproduce the action potential duration (APD) restitution of the Beeler-Reuter model for canine ventricular cells [13]. In the model the APD restitution curve is steep, and so a single spiral wave is unstable, and breaks up into multiple wavelet re-entry [18].

4 Results

The performance of the first method with various reference points and time-delay (*tau*) is illustrated in Fig.3 and Fig.4 for a 2D tissue simulation where a single spiral

wave has broken down into multiple wavelets 700 ms after initiation. The phase distribution in Fig.3 was obtained using (1). In Fig.4 white points label positive PSs (chirality = +1, clockwise rotation) and black negative PSs (chirality = -1, counter clockwise rotation).

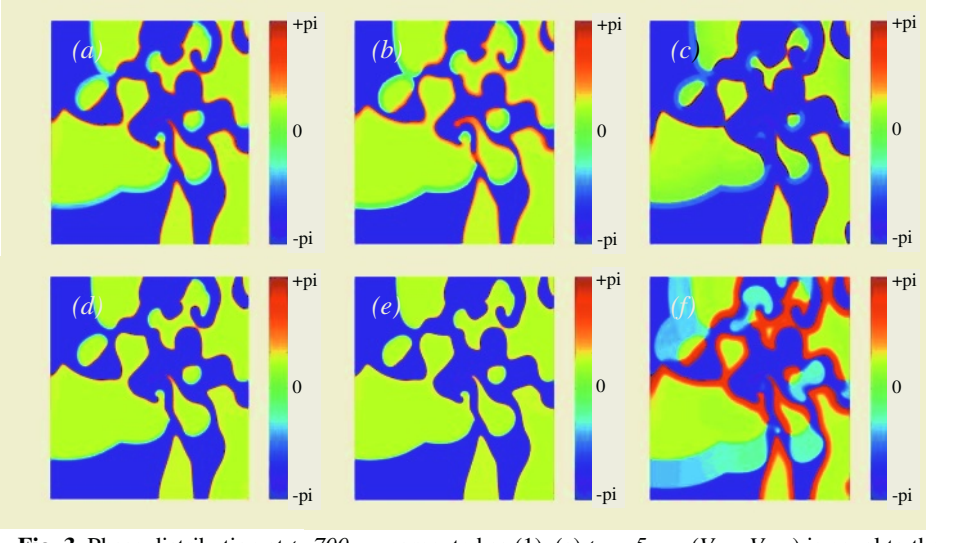

Fig. 3. Phase distribution at *t=700 ms* computed as (1). (a) *tau=5 ms*, ($V_{ref,x}$,$V_{ref,y}$) is equal to the mean value of $V_m(x,y,t)$ among all time records at the point *(x,y)*. (b) *tau=5 ms*, V_{ref} *=-65 mV*. (c) *tau=5 ms*, V_{ref} *=15 mV*. (d) *tau=2 ms*, V_{ref} =mean value of V_m . (e) *tau=1 ms*, V_{ref} =mean value of V_m . (f) *tau=25 ms*, V_{ref} =mean value of V_m

The phase distribution and PS location obtained using *tau* of 5 ms and three different ($V_{ref,x}$,$V_{ref,y}$) are shown in Fig.3(a)-(c) and in Fig.4(a)-(c) respectively. Although the overall phase distribution in each case is similar, there are two excess singularities in Fig.4(b) and three missing PSs in Fig.4(c) in comparison with Fig.4(a). Moreover, the coordinates of PSs obtained using 15mV as the reference point differ markedly from the coordinates of PSs in Fig.4(a) and 4(b).

Figures 3(d)-(f) and 4(d)-(f) demonstrate the change of phase distribution and PSs location with *tau,* which was equal to 2 (Fig.3(d), 4(d)), 1 (Fig.3(e), 4(e)), and 25 ms (Fig.3(f), 4(f)). Here the coordinates of the reference point were chosen as the mean value of $V_m(x,y,t)$. The PS location in Fig.4(a) and 4(d) are similar, but if *tau* is less then 2 ms (Fig.4(e)), there is an excess of singularities, similar to Fig.4(b). However, at *tau=25 ms* (Fig.4(f)) three PSs disappear similar to Fig.4(c).

The second technique for PS localization is illustrated in Fig.5, for the same 2D simulation. The figures represent contour plots of various V_{iso} : -10 mV (Fig.5(a)), -15 mV (Fig.5(b)), -20 mV (Fig.5(c)), -25 mV (Fig.5(d)), -30 mV (Fig.5(e)), -35 mV (Fig.5(f)). Blue snowflakes label PSs. PS location is strongly dependent on the choice of V_{iso}, and all parts of Fig.5 are different except Fig.5(e) and 5(f) which are similar and resemble Fig.4(b) and 4(e). Fig.5(c) is the exact copy of Fig.4(a) and 4(d). In some cases, very closely spaced PS pairs are identified and these are highlighted.

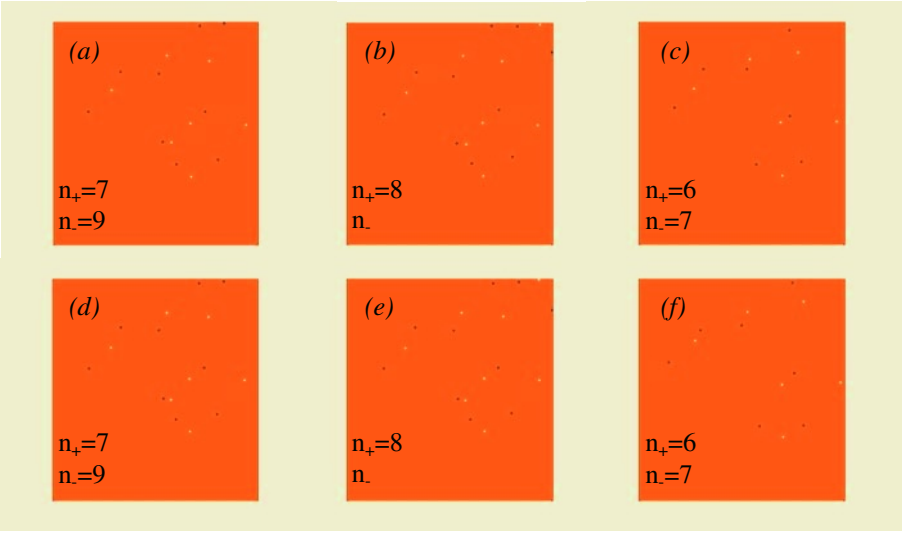

Fig. 4. Location of phase singularities corresponding to phase distribution in Fig.3. (a) *tau=5 ms*, ($V_{ref,x}$,$V_{ref,y}$) is equal to the mean value of $V_m(x,y,t)$ among all time records at the point *(x,y)*. (b) *tau=5 ms*, V_{ref} *=-65 mV*. (c) *tau=5 ms*, V_{ref} *=15 mV*. (d) *tau=2 ms*, V_{ref} =mean value of V_m . (e) *tau=1 ms*, V_{ref} =mean value of V_m . (f) *tau=25 ms*, V_{ref} =mean value of V_m

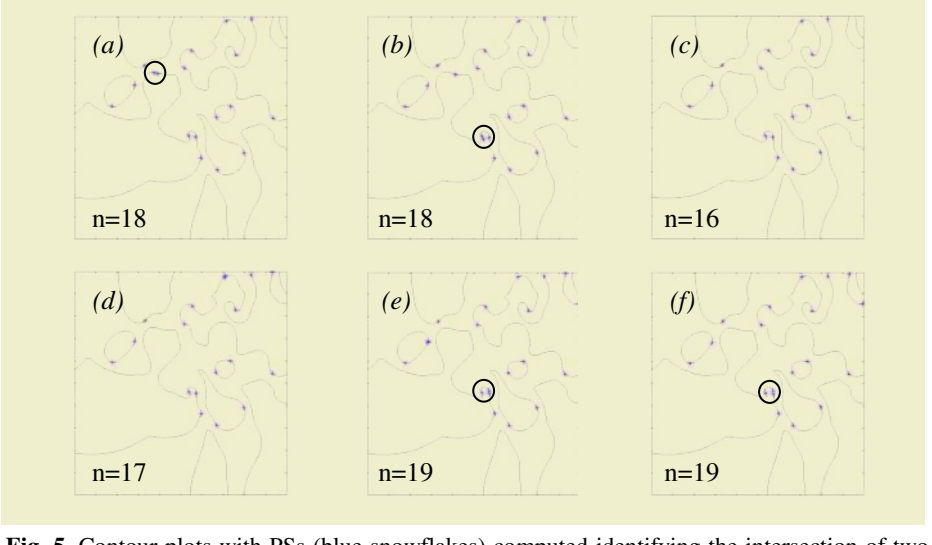

Fig. 5. Contour plots with PSs (blue snowflakes) computed identifying the intersection of two isolines at *t=700 ms*. (a) V_{iso}*=-10 mV*. (b) V_{iso}*=-15 mV*. (c) V_{iso}*=-20 mV*. (d) V_{iso}*=-25 mV*. (e) V_{iso}*=-30 mV*. (f) V_{iso}*=-35 mV*

A comparison of the two methods for PSs detection is presented in Fig.6. The distribution of membrane voltage with blue singularities obtained by the first method

is shown in Fig.6(a)-(c). Membrane voltage with PSs computed by the second technique is displayed in Fig.6(d)-(f). At *t=50 ms* a single spiral wave and one PS exist, and the PS is located correctly by both methods. Here *tau=5 ms* (Fig.6(a)) and V_{iso} *=-20 mV* (Fig.6(d)). It is clear that these two figures are identical. The example of a more complicated case is presented in Fig.6(b), 6(c), 6(e), 6(f). Here *t=600 ms*, *tau=5 ms* (Fig.6(b)), V_{iso} *=-20 mV* (Fig.6(e)), *tau=2 ms* (Fig.6(c)), V_{iso} *=-30 mV* (Fig.6(f)). The PS location computed using a time-delay of 5 ms is similar to location of singularities obtained by the second method with V_{iso} *=-20 mV*, and the PS coordinates computed by the first technique with *tau=2 ms* are almost the same as coordinates of singularities obtained using V_{iso} *=-30 mV*. However, there are some differences between the number of PSs identified, and these differences can be attributed to the closely spaced PS pairs that are circled in Fig.6(b) and 6(e).

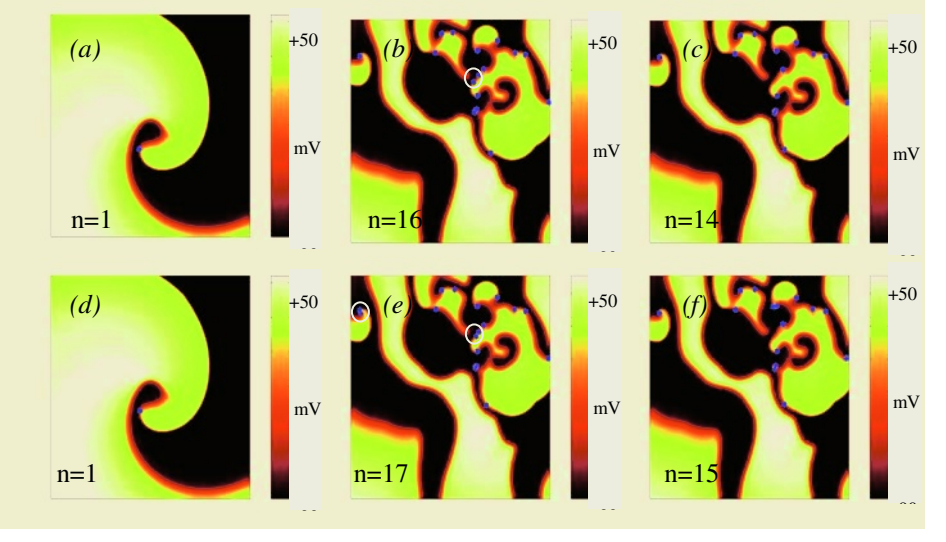

Fig. 6. Distribution of membrane voltage with singularities (blue snowflakes) obtained using both techniques for PSs detection. (a) *t=50 ms*, *tau=5 ms*, V_{ref} =mean value of V_m . (b) *t=600 ms*, *tau=5 ms*, V_{ref} =mean value of V_m . (c) *t=600 ms*, *tau=2 ms*, V_{ref} =mean value of V_m . (d) *t=50 ms*, V_{iso}*=-20 mV*. (e) *t=600 ms*, V_{iso}*=-20 mV*. (f) *t=600 ms*, V_{iso}*=-30 mV*

Trajectories of singularities computed by the first method with *tau=5 ms* and the mean value of membrane voltage as the reference point are displayed in Fig.7. Fig.7(a) shows PSs trajectories by 300 ms. By 111 ms a single positive (chirality=+1) PS (red trajectory) existed. At *t=111 ms* two additional PSs appeared: positive (yellow line) and negative (green) and a spiral wave began to break up. At 173 ms another two singularities were born: positive (magenta) and negative (black). At 175 ms the red and black PSs collided and disappeared. Continuing by a similar manner at 300 ms three singularities remained (a positive and two negative). However, at *t=1050 ms* the amount of positive PSs is a bit greater (Fig.7(b)). In Fig.7(b) red lines label trajectories of singularities of positive chirality and green – negative. In our

simulations all PSs were created in pairs (87 pairs of positive-negative singularities) or due to interaction with a boundary (5 PSs). The PSs vanished, either due to positive-negative collision (57 pairs) or by collision with a boundary (54 PSs).

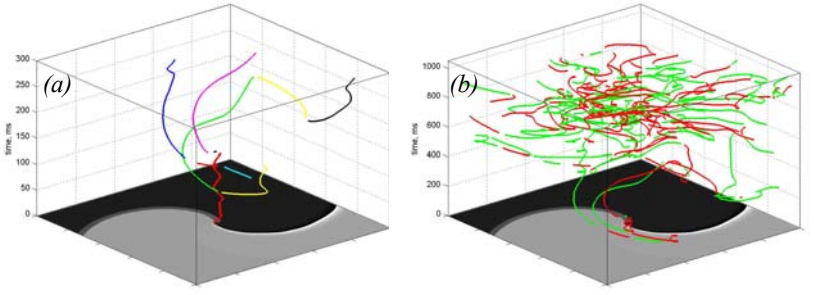

Fig. 7. PS trajectories computed using *tau=5 ms*, V_{ref} =mean value of V_m . (a) t ∈ [0; 300] ms. (b) t ∈ [0; 1050] ms. PSs trajectories of positive chirality are shown in red, trajectories of singularities of negative chirality are displayed in green

PS detection in 2D simulations of cardiac fibrillation. We have shown that both methods identify a broadly similar number of PSs, but the parameters used in each method can affect both the number of PSs that are detected as well as their location. PSs have already been identified in experimental data using the first method [7], and our study indicates that these results would be broadly comparable with the results of numerical studies where PSs are detected using the second technique.

The choice of *tau* and reference point is known to have a crucial influence on PS detection by the first method [8, 11, 14]. These values should be chosen such that the phase can be uniquely defined during the course of a spiral (scroll) wave rotation. The ideal reference point is one that is encircled by all trajectories independently of the originating spatial location. If one chooses a random point in the state space as the reference point, this point may lie within some trajectories and outside others. In this paper we compared the location of singularities obtained using the mean value of membrane voltage (that is supposed to be encircled by all trajectories) as the reference point (Fig. 4(a)), with PSs coordinates calculated using two example reference points.

As time-delay (*tau*) we chose four values, two of them (2ms and 25 ms) are often used in cardiac literature [8, 11, 14]. It was shown in [8, 11, 14] that for cardiac activation, if *tau* is on the order of the action-potential upstroke duration, the amount of trajectory folding (hence, nonunique calculation of phase) will reduce. Our results have demonstrated that assuming time-delay between 2 and 5 ms has a little effect (Fig.6(b), 6(c)) or no effect (Fig.4(a), 4(d)) on the PSs location. However, *tau* equal to 1 or 25 ms leads to additional or missing singularities relative to those obtained using *tau* of 5 ms and noticeable shift of PSs coordinates for time-delay of 25 ms.

Although an earlier study suggested that the choice of V_{iso} influences the location of the PS only slightly [19], our results have shown that this choice can be important (fig.5). The main effect is to identify additional closely spaced PS pairs.

The examples of *t=50 ms, t=600 ms* and *t=700 ms* (Fig.4-6) have demonstrated that using a time-delay of 5 ms in the first method for PSs detection produces a similar PS distribution to using V_{iso} *=-20 mV* in the second technique. In addition to the data shown in Fig.6, we also deployed each method at other times during the simulation. We found that if the number of PSs was insensitive to the choice of *tau* between 1 and 5 ms in the first method, then the choice of V_{iso} between –20 and -40 mV in the second method would also have little effect on the number of PSs detected. This finding suggests that the robustness of each method is variable, but a more systematic comparison of the two methods is needed.

The balance between created and destroyed PSs and the influence of boundaries are also topics for further investigation. Although our studies are preliminary, they indicate that the role of heart tissue boundaries could be important, especially for PSs death (54 singularities among 168 were destroyed due to collision with boundaries in spite of a quite large 12.5×12.5 cm domain), and hence these investigations could aid the development of possible defibrillation strategies.

6 Conclusions

In this paper we have compared two different methods for PSs detection, and using one of the techniques we have tracked singularities during the breakdown of a spiral wave into fibrillation (during approximately 1 s). Neither method is ideal since both require some parameter values to be chosen. However, there is clear advantage of using the first technique, which is based on topological charge. It immediately gives us knowledge about the sense of spiral wave rotation (chirality), and this is an additional feature that is extremely useful for PS tracking.

Acknowledgements

Ekaterina Zhuchkova is funded by INTAS fellowship 03-55-1920.

References

1. RA Gray, J Jalife: **Ventricular fibrillation and atrial fibrillation are two different beasts**. *Chaos* 1998, **8**:65-78.
2. J Jalife: **Ventricular fibrillation: Mechanisms of initiation and maintenance**. *Annual Review of Physiology* 2000, **62**:25-50.
3. JM Rogers, J Huang, WM Smith, RE Ideker: **Incidence, evolution, and spatial distribution of functional reentry during ventricular fibrillation in pigs**. *Circulation Research* 1999, **84**:945-954.
4. F Xie, ZL Qu, J Yang, A Baher, JN Weiss, A Garfinkel: **A simulation study of the effects of cardiac anatomy in ventricular fibrillation**. *Journal of Clinical Investigation* 2004, **113**:686-693.
5. PS Chen, TJ Wu, CT Ting, HS Karagueuzian, A Garfinkel, SF Lin, JN Weiss: **A tale of two fibrillations.** *Circulation* 2003, **108**:2298-2203.

6. AV Zaitsev, O Berenfeld, SF Mironov, J Jalife, AM Pertsov: **Distribution of excitation frequencies on the epicardial and endocardial surfaces of fibrillating ventricular wall of the sheep heart**. *Circulation Research* 2000, **86**:408-417.
7. RA Gray, AM Pertsov, J Jalife: **Spatial and temporal organization during cardiac fibrillation**. *Nature* 1998, **392**:75-78.
8. C Larson, L Dragnev, N Trayanova: **Analysis of electrically induced re-entrant circuits in a sheet of myocardium**. *Annals of Biomedical Engineering* 2003, **31**:768-780.
9. VN Biktashev, AV Holden, SF Mironov, AM Pertsov, AV Zaitsev: **Three-dimensional aspects of re-entry in experimental and numerical models of ventricular fibrillation**. *International Journal of Bifurcation and Chaos* 1999, **9**:695-704.
10. RH Clayton, AV Holden: **Filament behaviour in a computational model of ventricular fibrillation in the canine heart**. *IEEE Transactions on Biomedical Engineering* 2004, **51**:28-34.
11. AN Iyer, RA Gray: **An experimentalist's approach to accurate localization of phase singularities during re-entry**. *Annals of Biomedical Engineering* 2001, **29**:47-59.
12. M-A Bray, S-F Lin, RR Aliev, BJ Roth, JP Wikswo: **Experimental and theoretical analysis of phase singularity dynamics in cardiac tissue**. *Journal of Cardiovascular Electrophysiology* 2001, **12**:716-722.
13. F Fenton, A Karma: **Vortex dynamics in three-dimensional continuous myocardium with fibre rotation: Filament instability and fibrillation**. *Chaos* 1998, **8**:20-47.
14. M-A Bray, JP Wikswo: **Use of topological charge to determine filament location and dynamics in a numerical model of scroll wave activity**. *IEEE Transactions on Biomedical Engineering* 2002, **49**:1086-1093.
15. AT Winfree: **Varieties of spiral wave behaviour in excitable media**. *Chaos* 1991, **1**:303-334.
16. VN Biktashev, AV Holden: **Re-entrant waves and their elimination in a model of mammalian ventricular tissue**. *Chaos* 1998, **8**:48-56.
17. RH Clayton: **Computational models of normal and abnormal action potential propagation in cardiac tissue: Linking experimental and clinical cardiology**. *Physiological Measurement* 2001, **22**:R15-R34.
18. FH Fenton, EM Cherry, HM Hastings, SJ Evans: **Multiple mechanisms of spiral wave breakup in a model of cardiac electrical activity**. *Chaos* 2002, **12**:852-892.
19. RH Clayton, AV Holden: **A method to quantify the dynamics and complexity of re-entry in computational models of ventricular fibrillation**. *Physics in Medicine and Biology* 2002, **47**:225-238.